Ultrafast X-ray scattering reveals vibrational coherence following Rydberg excitation

Ultrafast X-Ray Scattering Reveals Vibrational Coherence Following Rydberg Excitation

Brian Stankus[1†], Haiwang Yong[1†], Nikola Zotev[2], Jennifer Ruddock[1], Darren Bellshaw[2], Thomas J. Lane[3], Mengning Liang[3], Sébastien Boutet[3], Sergio Carbajo[3], Joseph S. Robinson[3], Wenpeng Du[1], Nathan Goff[1], Yu Chang[1], Jason E. Koglin[3], Michael P. Minitti[3], Adam Kirrander[2], Peter M. Weber[1*]

[1] Department of Chemistry, Brown University, Providence, RI 02912, USA
[2] EaStCHEM, School of Chemistry, University of Edinburgh, David Brewster Road, Edinburgh EH9 3FJ, UK
[3] Linac Coherent Light Source, SLAC National Accelerator Laboratory, Menlo Park, CA, USA
*** Correspondence to: peter_weber@brown.edu**
† These authors contributed equally to this work.

Abstract:

The coherence and dephasing of vibrational motions of molecules constitute an integral part of chemical dynamics, influence material properties, and underpin schemes to control chemical reactions. In the present study, we measure coherent structural dynamics in optically excited N-methyl morpholine by scattering with ultrashort X-ray pulses from the Linac Coherent Light Source. The scattering signals are corrected for the different electron density in the excited electronic state of the molecule compared to the ground state. The experiment maps the evolution of the molecular geometry with femtosecond resolution, showing coherent motion that survives electronic relaxation and appears to persist for longer than previously seen using other methods.

The coherence of molecular vibrations, and its loss to dephasing, determines a wide array of molecular properties, and governs the widths and shapes of observed vibrational spectral lines[1,2]. Statistical theories for chemical reactions assume that dephasing leads to the dissipation of vibrational energy throughout the available phase space[3]. Dephasing thus is a challenge to the coherent control of chemical reaction dynamics using laser pulses[4] and to other fields relying on the quantum coherence of molecular vibrations. Recent spectroscopic studies have revealed that in N-methyl morpholine (NMM), coherent vibrational motions can survive an electronic relaxation process. This is an important discovery as such electronic relaxation phenomena in large molecule systems have traditionally been regarded as statistical in nature. Further explorations, ideally with complementary methods, are therefore imperative.

The advent of ultra-short pulsed optical lasers ushered in a new era of femtochemistry. Femtosecond laser pulses allowed for spectroscopic measurements of time-evolving molecules *in real time*, providing intriguing glimpses of the intricate ways in which molecular excitation can lead to chemical dynamics and vibrational coherences[5,6]. These ultrafast studies, relying on spectroscopic probes, have generated a wealth of knowledge about photochemical reaction mechanisms. Yet spectroscopy is an inherently indirect probe of structural dynamics, and following the dephasing of polyatomic molecules in real time, on the level of individual bond parameters, remains challenging.

With the recent advent of ultrafast X-ray Free-Electron Lasers (XFELs) and ultrafast electron diffraction (UED), more direct measurements of time-dependent atomic positions have become possible[7-15]. Ultrafast gas-phase scattering has emerged as a powerful tool for measuring molecular dynamics[7,8,13,14,16-18], revealing chemical reaction mechanisms that were previously inferred, but had not been observed. In the present study, we show that precise excited state

molecular structures can be obtained from X-ray scattering patterns and be used to construct a detailed picture of the dynamics with femtosecond time resolution. The low frequency vibrations of (NMM) were clearly resolved in space and time using time-resolved X-ray scattering with ultrafast pulses generated by the Linac Coherent Light Source (LCLS).

The analysis of the anisotropic X-ray scattering signal of NMM immediately following 200 nm excitation has previously revealed the population of the $3p_z$ molecular Rydberg state[19]. In ultrafast photoelectron spectroscopy studies, excitation to the $3p_z$ state has been seen to launch a coherent structural oscillation that persists following internal conversion to the 3s state with a 106 fs time constant[20]. Electronic structure calculations indicate that the molecular structure in the electronic ground state is a chair-equatorial structure[21,22] (shown in Figure 1), and the observed photoelectron signals indicate that the structural motion that is primarily responsible for the observed oscillation is a coherent vibration in a mode that involves the planarization of the amine, consistent with related computational studies on the same molecule.

In this work, the transient structures of the molecule at it evolves in time on the Rydberg surface are determined by matching the experimentally measured X-ray scattering patterns against a large set of computed patterns from a global geometry search in a conformational space created from molecular dynamics simulations. This analysis, along with a correction to the signals stemming from the change in electron density upon excitation, is capable of providing a femtosecond time-resolved determination of electronically excited molecular structures in a polyatomic molecule even in the absence of heavy elements.

In the experiment, a 200 nm UV pump pulse excites the molecules to the $3p_z$ Rydberg state[19,20] (Fig. 1). The scattering patterns created by intersecting the sample with a pulsed, 9.5 keV X-ray beam from the LCLS light source were detected by a 2.3-megapixel Cornell-SLAC

Pixel Array Detector (CSPAD)[23]. The positions of detected X-rays were converted to the coordinates of the scattering vector q and the azimuthal angle ϕ as described in the Supplementary Materials.

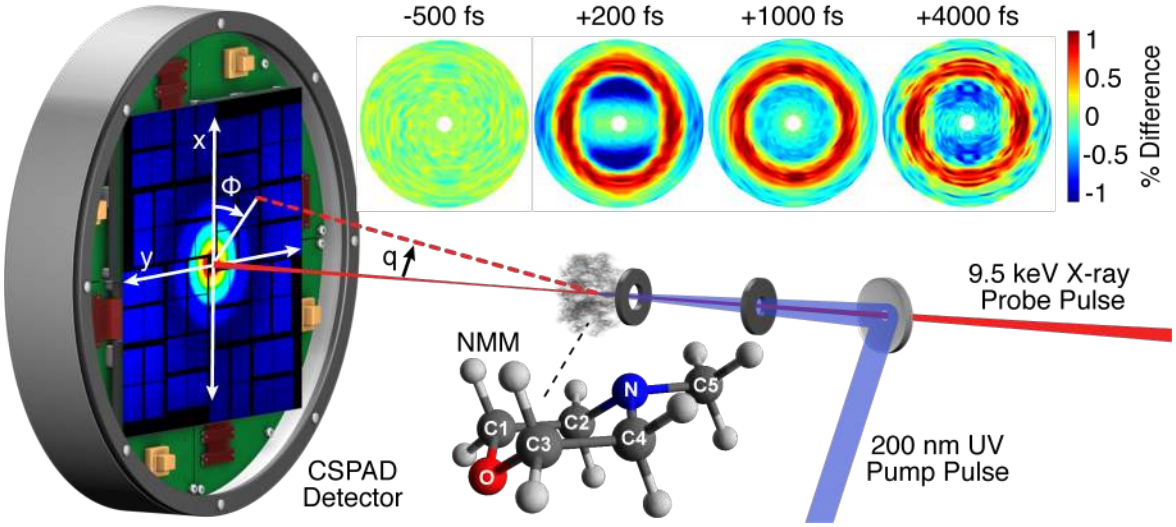

Fig. 1. A schematic of the experimental setup. The reaction of NMM is initiated with a 200 nm pump pulse, and the time-evolving molecular structure is probed via scattering using 9.5 keV X-ray probe pulses with variable time delay. The scattering signals are recorded with a CSPAD detector. The percentage change in the scattering pattern as a function of the momentum transfer vector (q) and azimuthal angle (Φ) for several representative time delays are also shown (top right).

Results and Discussion

The time-evolving signals are expressed as a percentage change, Eq. 1, where $I_{on}(\phi,q,t)$ represents the scattering pattern at the given time delay, and $I_{off}(\phi,q)$ is the scattering pattern of the ground state, un-excited molecules. The resulting time-dependent scattering images (see Fig. 1 for an illustration, a full animation is provided in Movie S1) show a sudden onset of the difference signal following the optical excitation. An anisotropic component of the signal, seen most clearly at t = 200 fs, arises from the preferential excitation of those molecules whose

transition dipole moments (TDM) are oriented parallel to the linear polarization of the optical pump pulse in the laboratory frame. Because the anisotropy is determined by the relationship between the TDM vector in the initially accessed state and the laser polarization vector, a detailed analysis of this component previously derived an unambiguous assignment of the initially excited state as the $3p_z$ Rydberg state[19]. The isotropic signal, on the other hand, contains all the intrinsic information of the molecule in the molecular frame, including both nuclear and electronic structural evolutions. The two components are decomposed from the two-dimensional scattering patterns using a standard method[24,25].

$$P_{diff}(\phi, q, t) = 100 \cdot \frac{I_{on}(\phi, q, t) - I_{off}(\phi, q)}{I_{off}(\phi, q)} \quad .\#(1)$$

The isotropic scattering signal, which shows a time dependence that reveals the dynamics of all internal degrees of freedom of the reacting molecule, has two main features: a rapid "step function" onset, and a subsequent oscillation that reflects vibrational motions in the molecule and occurs on a timescale in good agreement with previous photoelectron studies (623 ± 19 fs vs. 630 ± 13 fs measured before)[20]. (All errors are reported as 1σ.) The oscillation is heavily damped with a time constant of 635 ± 116 fs, which also agrees with the 530 ± 66 fs value measured via photoelectron spectroscopy. A third, low amplitude exponential decay feature (see Fig. S2 in Supplementary Materials) likely arises from intramolecular vibrational relaxation on a picosecond time scale. There is a rapid onset of the difference scattering signal that is attributed to the electronic transition of NMM from the ground state to the Rydberg state, as well as small-amplitude nuclear motions following electronic excitation. Consequently, in order to extract the structural motions of the vibrating molecule, the effect of the electronic excitation needs to be considered.

The effect on the scattering patterns resulting from the change in the electron density on account of the optical excitation is calculated using ab-initio multi-configurational wavefunctions obtained from the state-averaged complete active-space self-consistent field method (SA5-CASSCF(2,5)/6-311++G(d,p)).[26,27] Fig. 2 shows the effect on the scattering signals from electronic excitation compared to conformational change. The relative magnitude of the effect of the redistribution of electron density upon excitation is seen to be approximately half of the effect from the nuclear structure change, depending on the specific molecular geometry. At certain vibrational displacements, the two effects can be nearly comparable in magnitude, meaning that the signatures of both are captured in the scattering experiment. For example, for the planar structure represented in Figure 2, the electronic contribution has a magnitude of -5% difference at q = 1 $Å^{-1}$, while the structural contribution has a magnitude of only 2%. Clearly, the electronic contribution must be included to adequately account for the observed difference signals.

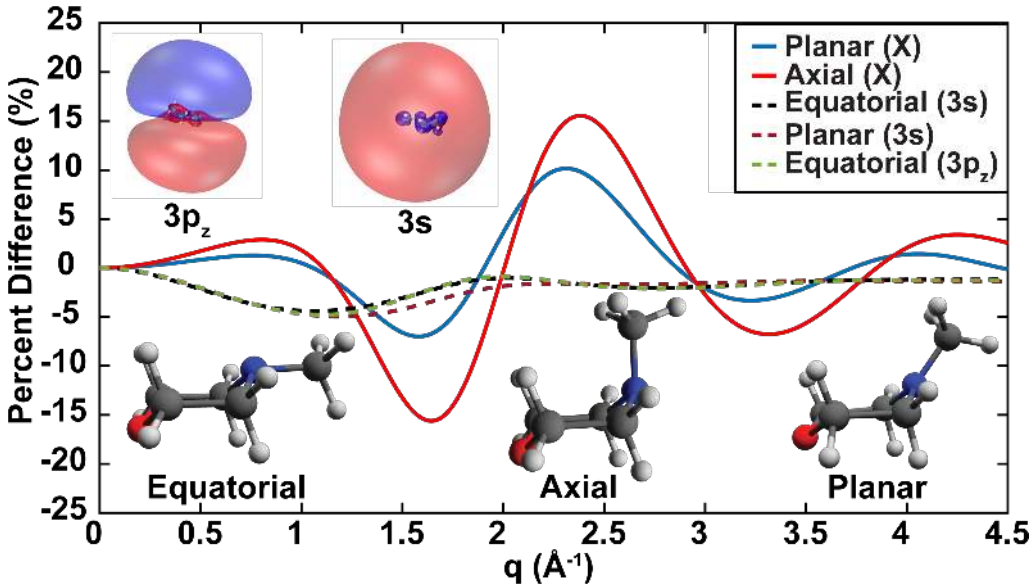

Fig. 2. Calculated percent difference scattering patterns caused by nuclear and electronic structure changes as a function of the momentum transfer amplitude *q*, assuming 100% excitation of the sample. The three relevant molecular conformations, as well as orbital plots for the 3s and $3p_z$ states, are included as insets. The "Planar (X)" curve (blue solid line) represents

the percent difference between the planar structure in the ground state and the equatorial structure in the ground state. The "Axial (X)" curve (red solid line) represents the percent difference between the axial structure in the ground state and the equatorial structure in the ground state. The "Equatorial (3s)" curve (black dashed line) represents the percent difference between the equatorial structure in the 3s state and the equatorial structure in the ground state. The "Planar (3s)" curve (red dashed line) is the percent difference between the planar structure in the 3s state and the planar structure in the ground state. The "Equatorial ($3p_z$)" curve (black dashed line) is the percent difference between the equatorial structure in the $3p_z$ state and the equatorial structure in the ground state.

The effect on the scattering signal arising from the change in the spatial distribution of the Rydberg electron as it internally converts from $3p_z$ to 3s is not experimentally observed, consistent with a very small difference in the calculated effect, Fig. 2. This is because the Rydberg orbitals are very diffuse and, when rotationally averaged, the difference between them is small. The electronic effect observed in the scattering experiment therefore must primarily arise from the vacancy left in the nitrogen valence orbitals of the tertiary amine group as an electron is promoted to the Rydberg orbitals. This also explains the observation in Fig. 2 that the electronic effect does not significantly depend on the geometrical structure of the molecule. Given that the all measured structural evolution occurs on the Rydberg manifold[20], the electronic contribution to the signal can be treated as approximately constant throughout the dynamics. As a consequence, it is possible to separate the electronic and nuclear effects on the scattering patterns and to treat their contributions to the signal as approximately additive.

In order to determine the transient molecular structures and construct the time-dependent movie of the dynamical motions, the experimental signal at each time point was compared against a large set of scattering patterns computed from many hypothetical structures. This large pool of possible structures was created by extracting structures from a large and diverse set of surface-hopping trajectories propagated on the ground and excited Rydberg electronic states with the excess kinetic energy from the excitation taken into consideration. Approximately one

million molecular geometries were extracted from the simulations. These geometries sample a large conformational space confined to energetically allowed conformations that could possibly be accessed by the molecule during the dynamics. For each molecular structure, a scattering pattern was computed by approximating the geometrical structure using the Independent Atom Model[28] and adding the contribution of the electronic excitation of the 3s state, planar structure (Fig. 2). By comparing the experimental signal with theoretical patterns, the least-squares fitting errors of all theoretical patterns from the pool were obtained at each time point. These errors were then plotted against each structural parameter, i.e. the interatomic distances and the bond angles. We found that in general, the least-squares error varies as a function of any given structural parameter in a normal or skewed-normal distribution. The peak centers of these distributions are taken to represent the best-fitting structural parameters (see further details in Supplementary Materials). This analysis gives the transient molecular structure at each time point independently, so that the measurement of many time points yields the time dependent motions of the excited-state molecule. In addition, the analysis results in the probability for the laser to excite the molecules to the upper electronic state. This global, time-independent parameter was determined to be 5.7%, a value that gives confidence that multi-photon excitation processes do not interfere with our analysis.

After the damping of the observed oscillations is complete, the difference scattering signals settle to an essentially constant value. Since the internal conversion from $3p_z$ to the 3s state is complete after ~0.5 ps, the scattering signal at long delay times arises from the structure of NMM in the 3s Rydberg state. The excited-state structure of NMM, determined from experimental signals at long delay time (2.6 to 3.9 ps), is given in Table 1. Because the determination of the molecular structure is performed independently for each of the 25 time

points, the structural parameters obtained from each of those time points are independent measurements that can be used to assess the precision of the structure determination. The errors reported in Table 1 are the standard deviations over measurements of independent time points. It is seen that the nearest-neighbor bond distances determined from this procedure have errors on the order of ~10 mÅ. To assess the accuracy of the result, Table 1 includes the optimized structure of NMM in its cation ground state. While the ion structure is not necessarily identical to the structure in the 3s Rydberg state, it is likely quite similar, and Table 1 shows a reasonable agreement. The most notable difference between the ion minimum energy structure and the vibrationally hot Rydberg excited state structure appears to be in the low frequency angular modes that likely are most affected by the high internal energy of the NMM molecule after internal conversion.

Table 1. Molecular structure parameters of vibrationally hot NMM in the excited 3s state, determined for delay times from 2.6 ps to 3.9 ps. Errors displayed are the standard deviations over measurements at different time points.

	Experimental: Rydberg-surface dynamics pool	Experimental: Ion-surface dynamics pool	Calculated Ion Structure	Calculated Ground-State Structure
Nearest-Neighbor Interatomic Distances (Å)				
O-C3	1.368 ± 0.005	1.373 ± 0.008	1.401	1.398
O-C1	1.364 ± 0.008	1.374 ± 0.006	1.401	1.398
N-C4	1.434 ± 0.012	1.449 ± 0.007	1.439	1.453
N-C2	1.441 ± 0.019	1.447 ± 0.009	1.439	1.453
N-C5	1.433 ± 0.007	1.430 ± 0.006	1.454	1.446
C3-C4	1.557 ± 0.009	1.554 ± 0.008	1.580	1.519
C2-C1	1.578 ± 0.023	1.552 ± 0.006	1.580	1.519
Characteristic Angles (°)				
C2-C1-C4-C3 Torsional	0.6 ± 1.5	-0.3 ± 0.5	0.0	0.0
O-N-C5 Umbrella	28.3 ± 6.1	20.4 ± 2.7	37.4	-24.1
N-C4-C2-C5 Pyramidalization	1.4 ± 1.2	-0.1 ± 1.0	4.0	-17.4
C5-N-C4-C3 Torsional	56.8 ± 4.3	44.3 ± 3.1	70.3	1.6

In order to ensure that the pool of possible molecular structures was sufficiently diverse, a second pool of structures was generated based on a combination of comparatively low-level DFT and Hartree-Fock classical trajectories propagated on the ground state of the cation of the molecule. Because the topology of the cationic state of the molecule is expected to be similar to that of Rydberg states of the neutral, the conformational spaces constructed from the two are expected to be similar. The results using this second pool, shown as "Experimental: Ion-surface dynamics pool" in Table 1, generally agree favorably with the high-level computation result ("Experimental: Rydberg-surface dynamics pool" in Table 1). The small discrepancy shown in torsional angles from two different pools is mainly due to the significantly smaller number of geometries used in the ion-surface dynamics pool compared to the Rydberg-surface dynamics pool (See details in Method section). This leads to a much lower local structure density around the true structure contained in the ion-surface pool compared to the Rydberg-surface pool. The consistency of the results obtained using the different pools demonstrates that the determination of molecular structures is robust with respect to the method used to generate the pool of structures. It should be noted, though, that because the calculated percent difference scattering pattern requires a simulated ground state scattering pattern as a reference, our method does depend on an accurate ground-state input structure. Given that the excited-state structure we determine is in good agreement with the calculated structure of the ground-state ion (Table 1), the ground-state input structure is inferred to be quite accurate.

Given the ability to determine precise excited state molecular structures for each time point, we are now in a position to assemble a graphical representation of the time dependent molecular structures, i.e. a molecular movie. For this illustration, the geometry that gives the smallest fit errors across all 21 non-hydrogenic interatomic distances is chosen as the

representative geometry. By stitching together the images at each time point, the dynamical motions of the vibrating molecule are obtained (animation is shown in Movie S2). An examination of the time dependence of some select structural parameters (Fig. 3) reveals the source of the dynamics observed in the experimental difference scattering pattern. Analysis of individual structural parameters indicates that the transient signal is dominated by signals arising from interatomic distances that involve the heavier atoms, rather than hydrogen atoms, and that change upon excitation: all the distances between C5 and the other heavy atoms, as well as the O–N distance. Selected representative time-dependent structural parameters are fitted to a dynamical model including the contributions described above. The O-N-C5 angle (refer to Fig. 1 for atom labels) has an oscillatory period of 619 ± 22 fs, while the C5-N-C4-C3 torsional angle oscillates with a 613 ± 14 fs period. Both of these values are in good agreement with the fits to the overall scattering signal oscillation period of 623 ± 19 fs, and the previous photoelectron spectroscopic measurement at 208 nm (630 ± 13 fs)[20]. This indicates that the primary driver of the observed oscillation is the planarization motion of the amine group. For comparison, Fig. 3 includes the time dependence of the C2-C1-C4-C3 torsional angle, which does not participate in this motion. This torsional angle is seen to remain essentially unchanged during the vibrational motion.

The time-dependent molecular structures also reveal that the oscillation in the O-N-C5 dephases with an exponential time constant of 1490 ± 785 fs, while the C5-N-C4-C3 torsional angle dephases in 1900 ± 876 fs. Both of these time constants are larger than the damping in the overall signal intensity, 635 ± 116 fs, although we note the relatively large errors in these determined values (see Supplementary Materials for details). This suggests that the decomposition of the overall scattering signals into specific, time-dependent geometrical

parameters allows a more comprehensive understanding of the oscillatory umbrella motion than direct dynamic analysis of the overall scattering signal. While the umbrella motion drives the relaxation of energy into the bath of vibrational states, its coherence may persist for longer than previously thought and than analysis of the overall signal intensity would suggest.

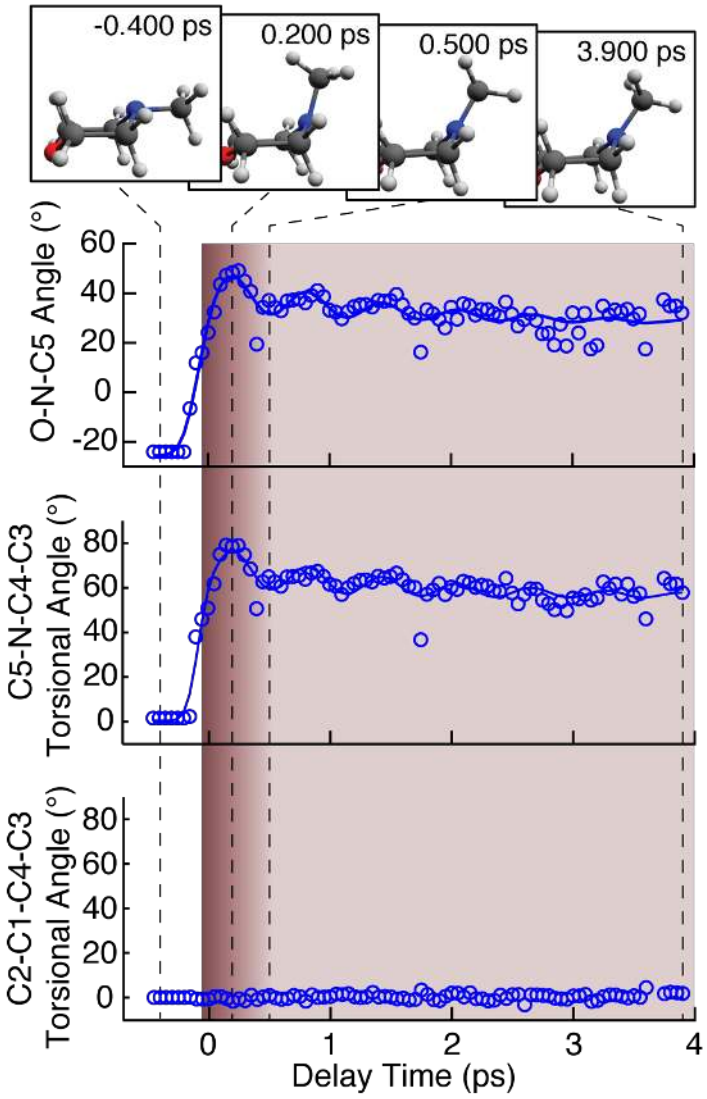

Fig. 3. Time-dependent plots of the O-N-C5 angle, the C5-N-C4-C3 torsional angle, and the C2-C1-C4-C3 torsional angle, extracted from the structural determination as described in the text, as well the dynamic fits to the respective vibrational motions of the O-N-C5 angle and the C5-N-C4-C3 torsional angle (solid lines). The approximate lifetime of the initially excited $3p_z$ Rydberg state (determined from photoelectron measurements in Ref. [20]) is shown as a dark red shaded region, which corresponds to the 3s state when the color is light pink. Example molecular structures for selected time points are also shown. A full animation as a molecular movie is given in the Movie S2.

Conclusions

In summary, we have captured transient molecular scattering signals that reveal the excited state molecular structures. Precise molecular structures are obtained by reference to a large pool of potential structures generated computationally, with the resulting structures shown to be robust with respect to the choice of computational method. The resulting time-dependent molecular structure uncovers the vibrational motions in an excited polyatomic organic molecule. We observe large amplitude vibrations of the amine planarization mode and its dephasing on a picosecond time scale. It appears that the coherence of the vibrational motion survives the electronic relaxation[20], and persists for multiple periods. While the overall signal intensity reflects the motions in many vibrational modes and therefore has a faster apparent dephasing, the time-dependence of specific structural parameters suggests that the intrinsic dephasing of the motions may be much slower than previously known.

The optical excitation in this instance is primarily a one-electron effect, and occurs on a background of the 56 electrons in the molecule. Because the scattering signals arise from the interference of scattering from different parts of the molecule, the excitation of a single electron leads to an effect on the scattering signal of about ~0.2% with the excitation fraction in the present experiment (Figure 2), which is well within the experimental detection limit of ~0.05%. Based on our study it is now conceivable that both vibrational structural motions and electron density changes can be observed during chemical reactions, opening the door to observe, in real time, the formation and destruction of chemical bonds. Application to a variety of chemical

reactions, including electrocyclic and charge transfer reactions, could provide previously unattainable experimental insights into chemical bonding and charge migration during reactions.

Methods

Experimental methods: The X-ray scattering measurements were performed in the CXI instrument[29] at the Linac Coherent Light Source[30] at the SLAC National Accelerator Laboratory. The 200 nm pump laser was the fourth harmonic of a 120 Hz Ti:Sa laser with an ~80 fs pulse duration and ~1 μJ/pulse on target, and a ~___ eV spectral bandwidth. The X-ray probe pulse was generated from LCLS operating at 120 Hz, with ~10^{12} photons/pulse at 9.5 keV photon energy with a ~30 fs pulse duration. The cross-correlation time of the pump and probe pulses was determined to be 89 ± 7 fs from the onset of the observed time-dependent scattering signals. The gaseous NMM sample pressure was controlled by a piezoelectric needle valve to ~7 torr of pressure at the interaction region. The gas cell and the CSPAD detector are in-vacuum, with an average background pressure outside the scattering cell of 2.6 x 10^{-4} torr, mostly comprised of NMM that flows out of the windowless scattering cell. The pulse energy and gas pressure were optimized for reduced background signal and <10% excitation probability. The interaction length is kept small at 2.4 mm, which prevents excessive Beer-Lambert attenuation of the UV beam at the downstream end of the interaction region.

In order to collect time-resolved scattering patterns, the pump-probe delay time was controlled by a motorized delay stage, and the shot-to-shot timing jitter of the X-ray beam was monitored with a specialized timing tool[31]. The actual time delay of each shot was then determined as the sum of the laser stage position and the time tool edge position. In addition, the shot-to-shot X-ray intensity was monitored by a photodiode downstream of the scattering cell. In order to achieve the necessary noise level (<0.1%), it was necessary to calibrate the intensity

after the diffractometer setup, since the X-ray also has spatial jitter that affects the transmission of the X-ray through the Pt pinholes (see Fig. 1).

The scattered X-rays were detected via a 2.3-megapixel Cornell-SLAC Pixel Array Detector (CSPAD)[23]. Details of the detector calibration, as well as the analysis of the measured scattering signals, are presented in the Supplementary Information of this work, as well as of reference 32.

Computational methods: To calculate the percent difference scattering signal caused by electronic excitation and by nuclear vibrational motions (see Fig. 2), the equatorial and axial geometries were optimized using the B3LYP/6-311++G(d,p) method for the neutral ground state, and the planar geometry was optimized using B3LYP/6-311++G(d,p) for the ionic ground state. The selected structural parameters of the optimized ionic ground state are shown in table 1, in the 'Calculated Ion Structure' column. The structure of the neutral ground-state equatorial geometry was further optimized at the CASSCF(2,5)/6-311+G(d) level, to be used for simulating the ground state scattering pattern as a reference. The selected structural parameters of the optimized neutral ground state are also presented in table 1, in the 'Calculated Ground-state Structure' column. The ab-initio wavefunctions used for simulating the scattering patterns in the 3s and 3p states were calculated using the SA5-CAS(2,5)/6-311++G(d,p) method at equatorial and planar NMM structures. All ab-initio calculations are performed using the MOLPRO electronic structure software package[33,34], and scattering patterns were calculated using our own computer codes documented in the following three references[26,27,35].

Using a total of 107 trajectories we obtained approximately one million molecular geometries. We simulate the Rydberg-surface dynamics of photoexcited NMM using the code SHARC[36,37,38] interfaced with MOLPRO. SHARC treats nuclear motions classically, but nonadiabatic effects are included using the fewest-switches surface-hopping approach. The

dynamics was propagated on the four lowest singlet electronic excitation states. The structures sampled from a Wigner distribution are initially populated to 3s and three 3p states based on their oscillator strengths, with 107 trajectories run for 1000 fs. The electronic structure calculations during the dynamics are run at the SA5-CAS(2,5)/6-311+G(d) level of theory. A pool of 1,070,107 (i.e. $>10^6$) geometries was extracted from the simulations. To test the dependence of the structure determination on the level of theory used, an ion-surface dynamics simulation was also performed. In this simulation, the nuclei are still treated classically, whereas electrons are treated quantum mechanically and calculated on the ion ground-state surface instead of the neutral Rydberg surfaces. We deliberately chose the ion surface rather than the Rydberg surface for this simulation as a further test of the independence of the resulting structure determination on the method used to create the pool of structures. In half of the trajectories, the UHF/6-311+G(d) method was used to calculate the ion state NMM at each time step, while in the other half of the trajectories, density functional theory using the PBE functional was used instead. Combined, 173,997 geometries were obtained by the ion-surface dynamics simulations. Further details of the structural determination are included in the Supplementary Information.

Data Availability

The raw experimental data are archived on SLAC's internal file system. The raw pools of computed structures are stored locally at Brown University. All raw data are available from the corresponding author upon reasonable request.

Code Availability

The calculation of elastic scattering patterns from ab-initio wavefunctions has been discussed in prior publications[26,27,35]. The codes used for calculating scattering patterns,

processing the experimental data, and the structural determination analysis are available from the corresponding author upon reasonable request.

Acknowledgements

The authors thank Greg Stewart (SLAC National Accelerator Laboratory) for his generous assistance with preparing figures. This work was supported by the U.S. Department of Energy, Office of Science, Basic Energy Sciences, under Award DE-SC0017995, and by the Army Research Office (Grant No. W911NF-17-1-0256). Use of the Linac Coherent Light Source (LCLS), SLAC National Accelerator Laboratory, is supported by the U.S. Department of Energy, Office of Science, Office of Basic Energy Sciences under Contract No. DE-AC02-76SF00515.

Author Contributions

PMW, AK, and MPM directed the project. ML and SB performed x-ray alignment and data collection. SC, JSR, and MPM performed laser alignment. TJL and JEK provided software support during the experiment. WD and YC performed record keeping during the experiment. BS, HY, NZ, JR, NG, YC, and WD performed analysis on the experimental data. HY, NZ, and DB performed theoretical computations and structural determination analysis. BS planned the detailed experiments and implemented the data analysis. BS and HY wrote the manuscript, in consultation with the other authors.

Competing Interests

The authors declare no competing interests.

References

[1] Heller, E. J. Bound-state eigenfunctions of classically chaotic hamiltonian systems: Scars of periodic orbits. *Phys. Rev. Lett.* **53,** 1515–1518 (1984).

[2] Tannor, D. J. *Introduction to quantum mechanics: a time-dependent perspective*. (University Science Books, 2007).

[3] Marcus, R. A. Electron Transfer Reactions in Chemistry: Theory and Experiment. *Angew. Chem. Int. Ed.* **32,** 1111–1121 (1993).

[4] Peirce, P., Dahleh, M. A. & Rabitz, H. Optimal control of quantum-mechanical systems: Existence, numerical approximation, and applications. *Phys. Rev. A* **37,** 4950 (1988).

[5] Zewail, A. H. Femtochemistry: Atomic-Scale Dynamics of the Chemical Bond Using Ultrafast Lasers (Nobel Lecture). *Angew. Chem. Int. Ed.* **39,** 2586–2631 (2000).

[6] Lambert, W. R., Felker, P. M. & Zewail, A. H. Quantum beats and dephasing in isolated large molecules cooled by supersonic jet expansion and excited by picosecond pulses: Anthracene. *J. Chem. Phys.* **75,** 5958–5960 (1981).

[7] Minitti, M. P. *et al.* Imaging Molecular Motion: Femtosecond X-Ray Scattering of an Electrocyclic Chemical Reaction. *Phys. Rev. Lett.* **114,** 1–5 (2015).

[8] Glownia, J. M. *et al.* Self-Referenced Coherent Diffraction X-Ray Movie of Ångstrom- and Femtosecond-Scale Atomic Motion. *Phys. Rev. Lett.* **117,** 153003 (2016).

[9] Küpper, J. *et al.* X-ray diffraction from isolated and strongly aligned gas-phase molecules with a free-electron laser. *Phys. Rev. Lett.* **112,** 1–6 (2014).

[10] Barty, A., Küpper, J. & Chapman, H. N. Molecular Imaging Using X-Ray Free-Electron Lasers. *Annu. Rev. Phys. Chem.* **64,** 415–435 (2013).

[11] Harb, M. *et al.* Electronically driven structure changes of Si captured by femtosecond electron diffraction. *Phys. Rev. Lett.* **100,** 1–4 (2008).

[12] Ischenko, A. A., Weber, P. M. & Dwayne Miller, R. J. Capturing Chemistry in Action with Electrons: Realization of Atomically Resolved Reaction Dynamics. *Chem. Rev.* **117,** 11066–11124 (2017).

[13] Yang, J. *et al.* Diffractive Imaging of Coherent Nuclear Motion in Isolated Molecules. *Phys. Rev. Lett.* **117,** 153002 (2016).

[14] Yang, J. *et al.* Imaging CF_3I conical intersection and photodissociation dynamics with ultrafast electron diffraction. *Science.* **361,** 64–67 (2018).

[15] Zewail, A. H. 4D Ultrafast Electron Diffraction, Crystallography, and Microscopy. *Annu. Rev. Phys. Chem.* **57,** 65–103 (2006).

[16] Budarz, J. M. *et al.* Observation of femtosecond molecular dynamics via pump – probe gas phase x-ray scattering. *J. Phys. B At. Mol. Opt. Phys.* **49,** 34001 (2016).

[17] Minitti, M. P. *et al.* Toward structural femtosecond chemical dynamics: imaging chemistry in space and time. *Faraday Discuss.* **171,** 81–91 (2014).

[18] Williamson, J. C., Cao, J., Ihee, H., Frey, H. & Zewail, A. H. Clocking transient chemical changes by ultrafast electron diffraction. *Nature* **386,** 159–162 (1997).

[19] Yong, H. *et al.* Determining Orientations of Optical Transition Dipole Moments Using Ultrafast X-ray Scattering. *J. Phys. Chem. Lett.* 6556–6562 (2018). doi:10.1021/acs.jpclett.8b02773

[20] Zhang, Y., Jónsson, H. & Weber, P. M. Coherence in nonradiative transitions: internal conversion in Rydberg-excited N-methyl and N-ethyl morpholine. *Phys. Chem. Chem. Phys.* **19,** 26403–26411 (2017).

[21] Zhang, Y., Deb, S., Jónsson, H. & Weber, P. M. Observation of Structural Wavepacket Motion: The Umbrella Mode in Rydberg-Excited N-Methyl Morpholine. *J. Phys. Chem. Lett.* **8,** 3740–3744 (2017).

[22] Waters, M. D. J. *et al.* Symmetry controlled excited state dynamics. *Phys. Chem. Chem. Phys.* **21,** 2283–2294 (2019).

[23] Philipp, H. T., Hromalik, M., Tate, M., Koerner, L. & Gruner, S. M. Pixel array detector for X-ray free electron laser experiments. *Nucl. Instruments Methods Phys. Res. Sect. A Accel. Spectrometers, Detect. Assoc. Equip.* **649,** 67–69 (2011).

[24] Baskin, J. S. & Zewail, A. H. Ultrafast electron diffraction: Oriented molecular structures in space and time. *ChemPhysChem* **6,** 2261–2276 (2005).

[25] Lorenz, U., Møller, K. B. & Henriksen, N. E. On the interpretation of time-resolved anisotropic diffraction patterns. *New J. Phys.* **12,** (2010).

[26] Northey, T., Zotev, N. & Kirrander, A. Ab initio calculation of molecular diffraction. *J. Chem. Theory Comput.* **10,** 4911–4920 (2014).

[27] Northey, T., Moreno Carrascosa, A., Schäfer, S. & Kirrander, A. Elastic X-ray scattering from state-selected molecules. *J. Chem. Phys.* **145,** (2016).

[28] Warren, B. E. *X-ray Diffraction*. (Courier Corporation, 1969).

[29] Liang, M. *et al.* The Coherent X-ray Imaging instrument at the Linac Coherent Light Source. *J. Synchrotron Radiat.* **22,** 514–519 (2015).

[30] Emma, P. *et al.* First lasing and operation of an ångstrom-wavelength free-electron laser. *Nat. Photonics* **4,** 641–647 (2010).

[31] Bionta, M. R. *et al.* Spectral encoding method for measuring the relative arrival time between x-ray/optical pulses. *Rev. Sci. Instrum.* **85,** (2014).

[32] Ruddock, J. M. *et al.* Simplicity beneath Complexity: Counting Molecular Electrons Reveals Transients and Kinetics of Photodissociation Reactions. *Angew. Chemie - Int. Ed.* (2019). doi:10.1002/anie.201902228

[33] Werner, H. J. *et al.* MOLPRO, version 2012.1, a package of ab initio programs. *see http//www. molpro. net* (2012).

[34] Werner, H. J., Knowles, P. J., Knizia, G., Manby, F. R. & Schütz, M. Molpro: A general-purpose quantum chemistry program package. *Wiley Interdiscip. Rev. Comput. Mol. Sci.* **2,** 242–253 (2012).

[35] Moreno Carrascosa, A., Northey, T. & Kirrander, A. Imaging rotations and vibrations in polyatomic molecules with X-ray scattering. *Phys. Chem. Chem. Phys.* **19,** 7853–7863 (2017).

[36] Mai, S. *et al.* SHARC2.0: Surface Hopping Including Arbitrary Couplings — Program Package for Non-Adiabatic Dynamics. (2018).

[37] Mai, S., Marquetand, P. & González, L. Nonadiabatic dynamics: The SHARC approach. *Wiley Interdiscip. Rev. Comput. Mol. Sci.* 1–23 (2018). doi:10.1002/wcms.1370

[38] Richter, M., Marquetand, P., González-Vázquez, J., Sola, I. & González, L. SHARC: Ab initio molecular dynamics with surface hopping in the adiabatic representation including arbitrary couplings. *J. Chem. Theory Comput.* **7,** 1253–1258 (2011).